Nucleate pool boiling of demineralized water and acetone on smooth and roughened surfaces of aluminum alloy

R. M. Abd El–Aziz, M. H. Sakr, M. F. Abd Rabbo and A. H. Khalifa
[a] *Mechanical. Eng. Dept., Shoubra Faculty of Eng., Zagazig University, Cairo, Egypt*

In this research work, an experimental study was performed on the effects of surface condition and boiling liquid combinations on the heat transfer performance of the heated surface during saturated nucleate pool boiling. To meet the aforementioned needs, a pool boiling test apparatus was designed and constructed to achieve heat transfer measurements from seven horizontal upward facing aluminum alloy 6061 plates. These tested plates were: mirror finish, three mechanically treated surfaces and three chemically treated surfaces. All surfaces are tested in pools of saturated demineralized water and acetone for free convection and isolated bubble regimes. Tests showed that the enhancement in the nucleate pool boiling heat transfer coefficient reached up to 600% due to the variation in the roughness of the heated surface. From pool boiling heat transfer data, the size distribution function of stable vapor bubbles in active nucleation sites for each one of the seven heated surfaces was deduced. Finally, the size distribution function constants were correlated with the surface roughness parameter (R_P).

يدرس هذا البحث تأثير الحالة السطحية لسطح غليان أفقي مصنع من سبيكة الألمنيوم ٦٠٦١ على الأداء الحراري لسطح الغليان أثناء الغليان الحر لماء المفاعل وسائل الأسيتون عند الضغط الجوى كل على حدة. ولدراسة أهداف البحث, تم تصميم وبناء تختة اختبار تسمح بإجراء جميع القياسات الحرارية للغليان الحر باستخدام سبعة أسطح غليان أفقية تتضمن سطح أملس (مرآة) وثلاثة أسطح معالجة ميكانيكيا باستخدام أوراق صنفرة مختلفة فى درجات الخشونة بحيث تعطى خشنات متدرجة للأسطح وثلاثة أسطح أخرى معالجة كيميائيا باستخدام محلول الهيدروكلوريك بتركيز ثابت وزمن معالجة مختلف من سطح لأخر.وقد نم إجراء التجارب العملية عند الضغط الجوى للغليان الحر على الأسطح كل على حدة باستخدام مائعي التشغيل: ماء المفاعل وسائل الأسيتون.وقد أثبتت النتائج وجود تحسن مقداره ٦٠٠% فى معامل انتقال الحرارة أثناء الغليان الحر نتيجة تغيير الحالة السطحية لسطح الغليان. كذلك تم حساب الدالة التوزيعية للتكهفات الموجودة على كل سطح غليان مختبر باستخدام قياسات انتقال الحرارة. وباستخدام هذه الدوال التوزيعية تم حساب الثوابت الثلاثة المميزة لكل سطح غليان مختبر وأمكن أيجاد العلاقة بين هذه الثوابت ومتغير الخشونة للسطح المختبر.

Keywords: Nucleate pool boiling, Conditions of boiling surface, Size distribution function, Bubble flux density

1. Introduction

An understanding of the factors that influence the onset of boiling is of importance in the design and operation of cooling systems associated with high heat flux units. Data from other substances have demonstrated that nucleate boiling is generally influenced to a greater extent by surface condition than film boiling. Unfortunately, in many engineering problems, the nucleate pool boiling heat transfer cannot be determined analytically but must be evaluated experimentally.

Jakob [1] indicated qualitatively that for a given superheat, the rate of heat transfer is increased by increasing the microscopic roughness. The experimental studies of Berenson [2], Danilowa et al. [3] and Danilowa [4], among many, provided quantitative experimental data concerning the significance of the surface finish effect with various fluid-surface combinations on heat transfer. In particular, Berenson reported a change ranged from 500 to 600% in the nucleate boiling heat transfer coefficient due to variation in surface roughness. Corty and Foust [5, 6] were among the pioneers to investigate the role of surface conditions in nucleate boiling. They boiled ether and n-pentane from polished nickel and copper surfaces. The surfaces were prepared using emery papers to have a roughness parameter (*rms*) ranged from 2.2 to 23 μm.

Steeper slopes for heat transfer coefficient versus superheat were found. They indicated qualitatively that for a given superheat, the rate of heat transfer increased as the microscopic roughness increased. None of the many models for predicting rates of nucleate boiling heat transfer has been able to incorporate this effect since the nucleate characteristics of a surface are relatively sensitive to the surface micro-roughness measured by a profilometer. The experimental results of Tanes [7] indicated that the influence of surface roughness on the heat transfer coefficient cannot be described by a single roughness parameter in the form of simple relation $(h \sim (R_p)^n$ or $h \sim (R_z)^n)$ within an extended range of heat flux and saturation pressure and for surfaces with different forms of treatment e.g. mechanical or chemical. Moreover, the experimental and theoretical results of Salem [8] indicated that it is possible to describe pool boiling heat transfer data for different surface properties by a three-parametric distribution function $N(r)$ of the size of stable bubbles in active nucleation sites of the heated surface although only approximate expressions for the bubble frequency f and the bubble diameter D_b were used in the calculation of $N(r)$. He developed an expression to predict the relation between the heat transfer coefficient h and the active nucleation site density in the form:

$$\frac{h - h_{nc}}{h_{nuc} - h_{nc}} = \frac{N}{A}.\pi D_b^2 . \qquad (1)$$

Anderson et al. [9] were able to represent their data together for boiling of five different fluids on a glass surface into a single curve of active site density (N/A) versus the parameter group $(2\sigma T_s / \rho_v h_{fg} \Delta T)$. Gaertner [10] developed an expression to predict the nucleation site density in the form:

$$(N/A) = \left(\frac{N_o}{A}\right).exp(-k/T_w^3) , \qquad (2)$$

where k is a function of the fluid properties and surface condition. Brown [11] investigated bubble nucleation from different surfaces with various surface finish. One distinguishing feature of Brown's work was the fact that the number of active sites per unit area $(N/A)_{rc}$ with radii larger than r_c was correlated by the power law:

$$(N/A)_{rc} = C\,(1/r_c)^m , \qquad (3)$$

where $(N/A)_{rc}$ is the active site density of those cavities having radius equal to or greater than r_c, C and m are constants characterizing the boiling surface. Recently, Hsieh et al. [12] developed nucleate pool boiling correlation for five different rib-type roughened tube geometry (including plain tube) with different rib angles of 30°, 45°, 60° and 90° for both distilled water and R-134a as the working media. Bubble departure diameter, frequency of bubble emission and the active nucleate site density with the influence of the rib angle for this type of roughened surface were obtained. Boiling heat flux incorporating natural convection, nucleate boiling and micro-layer evaporation mechanisms following Benjamin and Balakrishnan [13] was predicted. Heat transfer correlation was also developed in terms of the degree of superheat and active nucleation site density. The dependence for these two parameters was found in favorable agreement with that of previous study for smooth surfaces.

The objective of this paper is to enlarge the pool boiling data base for alternative refrigerants by providing heat transfer data for deminerlized water and acetone from a variety of horizontal upward facing smooth and roughened enhanced surfaces and, furthermore, to develop a correlation between the size distribution function constants and the surface roughness parameter R_P measured directly by a profilometer.

2. Experimental set-up and procedure

2.1. Test facility and test section

The experimental apparatus used in the present study is shown in fig. 1. It consists of a cylindrical steel pressure vessel (evaporator) 194mm inner diameter, 220mm outer diameter and 300mm height. It is provided with two glass windows facing each other at a level 150 mm from the bottom for visualization. The heated surface test plate is fixed at the bottom

flange so that the heating surface is located 20mm lower than the center line of the glass windows. At the entrance section to the evaporator, the temperature of the condensate is raised to the saturation temperature of the boiling liquid (demineralized water or acetone) inside the evaporator, by continuously adjusting the power input to the electric heater connected to the condensate line before entry to the evaporator. A layer of polyurethane 50mm thickness and 40 kg/m^3 density covered by aluminum foil thermally insulates the evaporator.

A shell-and coil condenser is mounted above the evaporator and inclined at 15° to the horizontal. The shell is a cylindrical stainless steel tube 100 mm inner diameter, 104 mm outer diameter and 550 mm length. A polyurethane layer with aluminum foil thermally insulates the shell. The coil is a copper tube 10.5 mm inner diameter, 12.7 mm outer diameter and 6000 mm length. A thermo-static water storage tank of 50-liter capacity is used to supply water at the desired temperature to the condenser. Vapor refrigerant enters the shell naturally from the top through which it condenses and leaves the shell from the bottom by gravity.

Fig. 2 shows the details of the tested plates. It consists of a heating element made from a copper rod 36 mm diameter and 130 mm length. A one-millimeter thickness mica sheet electrically insulates the copper rod. A Nickel-Chrome electric resistance 1 mm diameter, 940 mm length and 1.6 ohm/m, is then wrapped around the copper rod. The maximum power output of the copper rod assembly is 3.5 kW. The copper rod assembly is then screwed with a copper disc 36 mm inner diameter, 58 mm outer diameter and 30 mm height. This copper disc is used as a base for the aluminum alloy 6061 test plate specimens. One of seven test plate specimens is assembled with the copper disc by a stainless steel nut 68 mm inner diameter and 86 mm outer diameter. The stainless steel nut is screwed on a stainless steel flange 58 mm inner diameter, 140 mm outer diameter and 26 mm thickness. The stainless steel flange is welded with the steel flange . Glass wool thermally insulates the heater element to minimize the heat loss to the surroundings. The input power to the Nickel-Chrome electric resistance is supplied from the power leads through a variac. The input power is calculated from separate measurements of the voltage between the power leads and the current, using a digital clip-meter (KYORITSU 1250831 & ± 0.1 A, ± 0.1 V accuracy).

The temperature of the heated surface (aluminum alloy 6061 test plate) is measured by means of four calibrated copper-constantan thermocouples. The hot junctions of these thermocouples are fixed at the bottom of the aluminum test plate through four radial drilled holes using an instant adhesive epoxy. These holes are machined at different lengths and at right angles as shown in fig. 3. The average upper surface temperature is obtained by extrapolating the above four measured values up to the heated surface. The liquid temperature in the evaporator is measured by two thermocouples of the same type placed close to the free surface of the liquid. Another two thermocouples are used to measure the vapor temperature and are positioned midway along the evaporator, about 15 mm above the liquid surface. A compensated temperature indicator (model T/S 4000/3000 with ± 0.5 °C accuracy) receives the emf of all thermocouples through a selector switch. A calibrated bourdon tube pressure gauge (0-3 bar) is used to indicate the system pressure. It is fixed at the charging line of the evaporator. A hand valve connecting the charging bottle of either the demineralized water or the acetone through a test manifold.

2.2. Preparation of the test plate specimens

In the present study, the surfaces of the test plates were so treated so as to produce a variety of surface roughness. Seven aluminum alloy 6061 plates having the same dimensions were used as the heating surfaces during the pool boiling experiments. These plates were firstly polished to mirror finish using fine grade emery papers (500, 600, 800, 1000, 1200 & 1500 grades) together with polishing powder. Once the surface finish was completed, the plates were cleaned with acetone and rinsed with distilled water. Next, the surface of the plates was tested for its roughness parameter with a surface profilometer. Secondly, the surface of the plates (hereinafter denoted by S2, S3 and S4) were re-treated

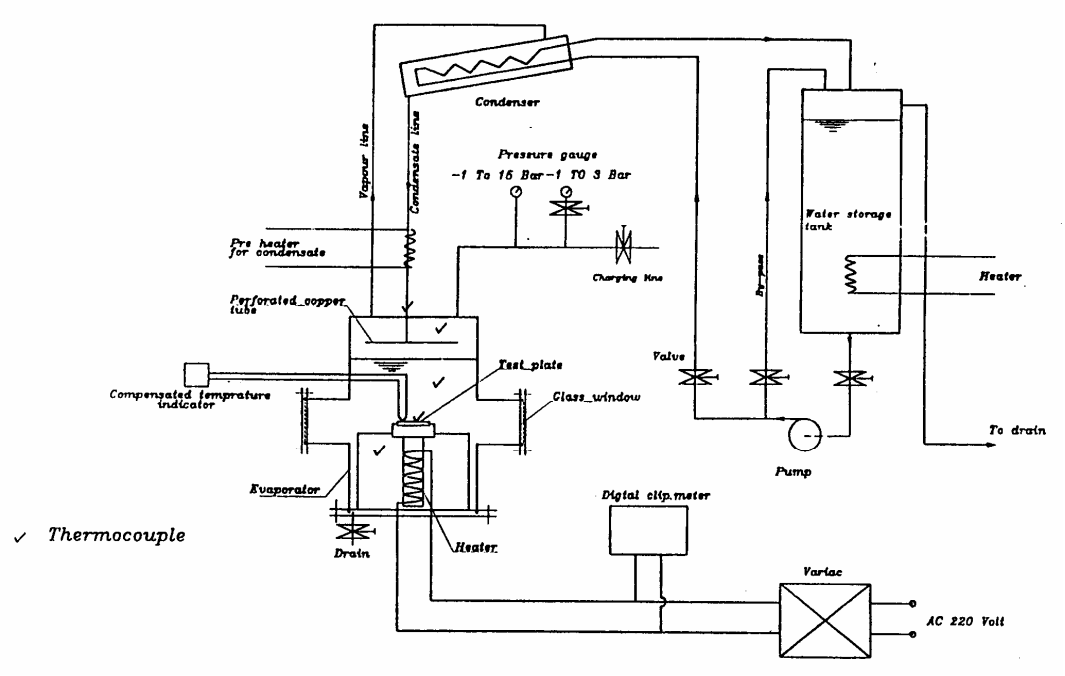

Fig. 1. Line diagram of the test apparatus.

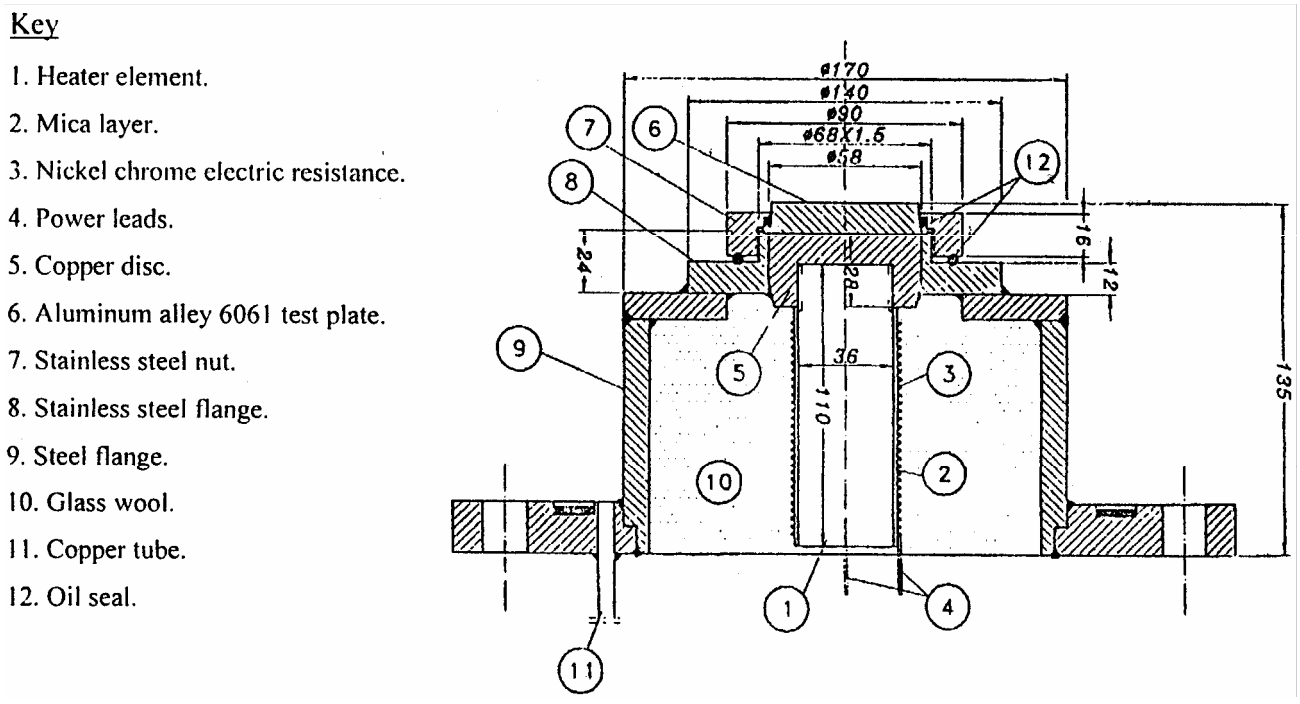

Fig. 2. Details of the boiling surface assembly.

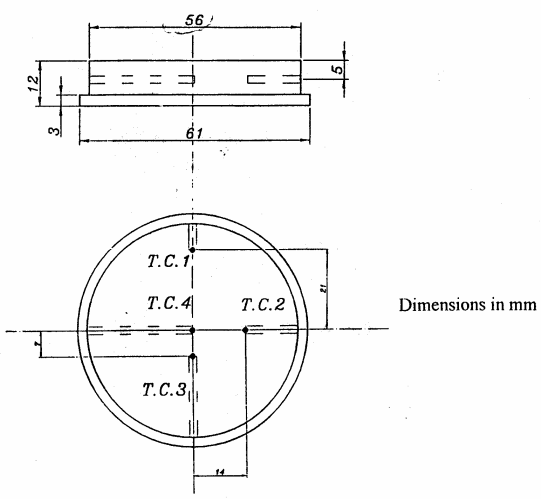

Fig. 3-a. Location of the thermocouples.

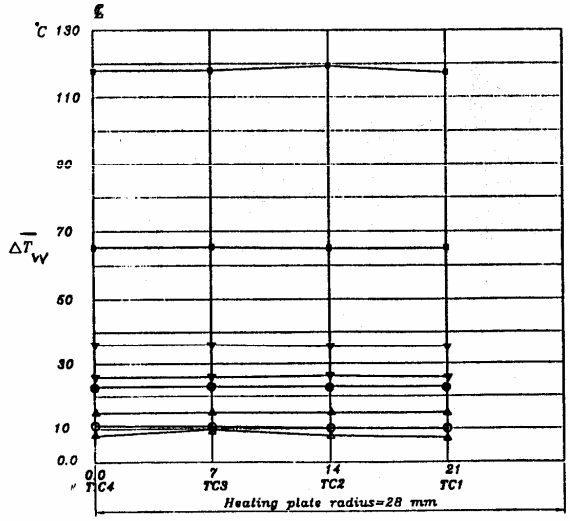

Symbol	Plate No.	B.liquid	q(W/m²)	$\Delta\overline{T}_w$ °C
□	S1	Acetone	246639	118.166
■	S1	Water	300920	65.166
▽	S7	Acetone	255784	36.67
▼	S7	Water	316242	26.08
●	S1	Acetone	31226	23.00
▲	S1	Water	41087	16.00
○	S7	Acetone	31809	10.50
△	S7	Water	49628	8.25

Fig. 3-b. Radial variation of the excess temperature $\Delta\overline{T}_w$ of the boiling surface at higher and lower values of ΔT and heat flux.

mechanically by using different coarse emery papers with 280, 100 and 24 grades respectively. On the other side, the surface of the plates (hereinafter denoted by S5, S6 and S7) were re-treated chemically, where the corrosion potential for the aluminum alloy 6061 was measured in a time period of 900 seconds using saturated calomel electrode (SCE) as a reference electrode in 2M HCL. The maximum potential after 900 seconds was 1.47 V. At this potential the aluminum alloy 6061 tested plates were potentio statically polarized by electrical impedance analyzer model 6010 in 2M HCL for different times namely 350, 450 and 550 seconds, to get a variety of pit densities at the surfaces (S5, S6 and S7). Once the mechanical and chemical treatments were completed, the surface of the seven tested plates were cleaned with acetone, rinsed with distilled water and dried by the supply of hot dry air. Next these surfaces were tested for its roughness parameter (R_P) defined by DIN 4762 standards using a surface profilometer. Fig. 4 shows typical segments taken from the recorder traces of the profilometer for the surfaces of the seven tested plates. On the other side, in order to get further information about the structure of the tested plates, photographs were taken with an optical scanning microscope as shown in fig. 5.

2.3. Experimental procedure

Before each test run, the evaporator and the first surface of the seven tested plates were rinsed well with distilled water and dried by a supply of hot dry air. After that, the plate surface was assembled with the clean evaprator. The system was then evacuated to a pressure of about 0.03 bar. If no leaks were detected over a 24 hour interval, the evaporator was charged with the boiling liquid (either demineralized water or acetone) from the reservoir to a level 100 mm above the heating surface.

In order to remove the air from the system, boiling was started at a pressure of 0.7 bar from the heating surface at the maximum heat flux furnished by the electric heater (250 kW/m^2) for 3.5 hours before the heat transfer coefficient would become constant with time.

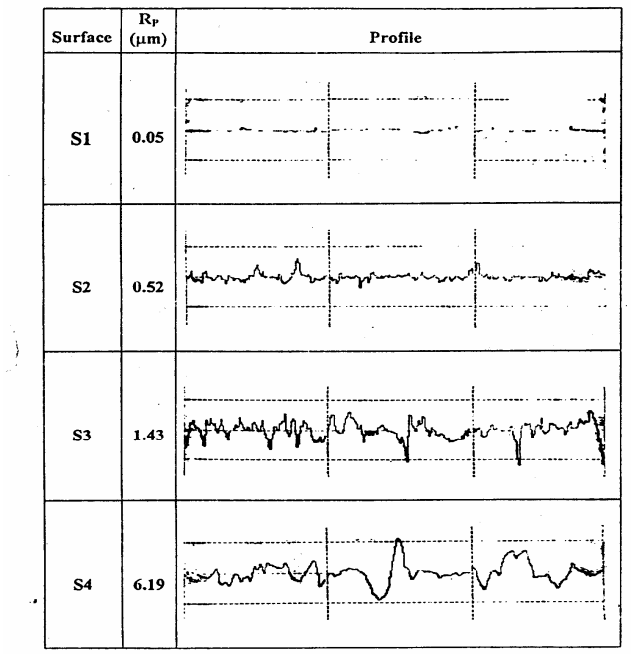

Fig. 4-a. Typical segments taken from the recorded traces of the profilometer for the mechanically treated surface (S1, S2, S3 & S4).

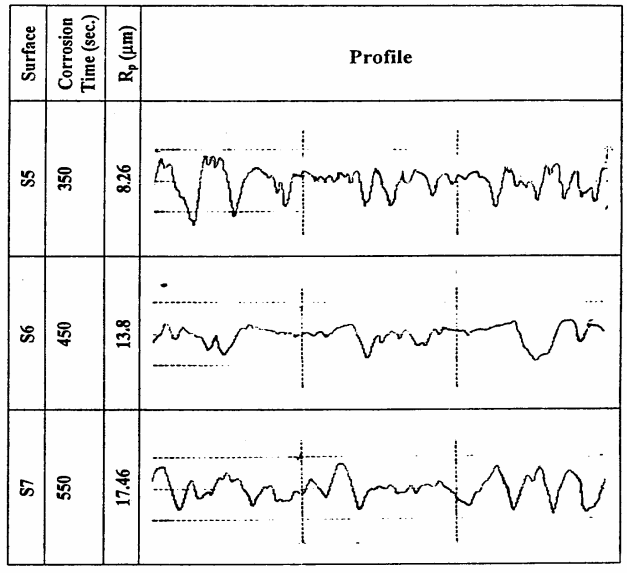

Fig. 4-b. Typical segments taken from the recorded traces of the profilometer for the chemically treated surface (S5, S6 & S7).

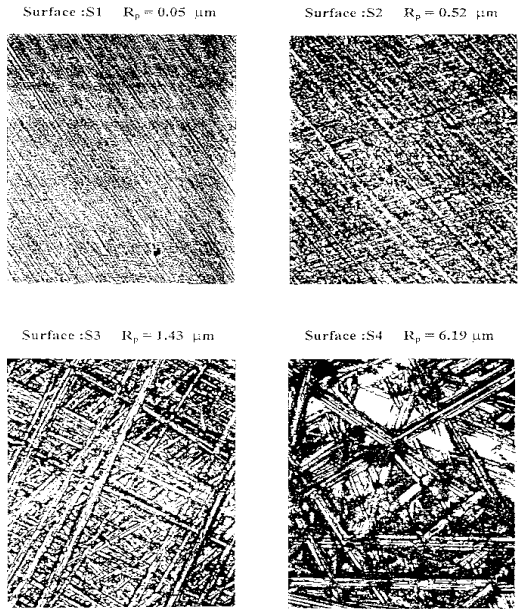

Fig. 5-a. Pictures taken from the optical microscope for the mechanically treated surface (S1, S2, S3 & S4).

Surface	Corrosion time (sec.)	Rp (μ_m)	Picture
S5	350	8.26	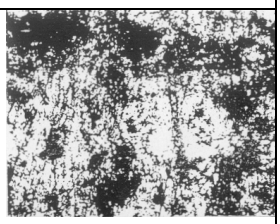
S6	450	13.8	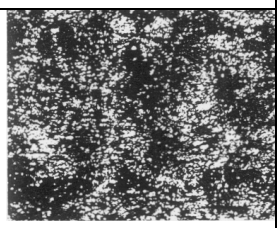
S7	550	17.46	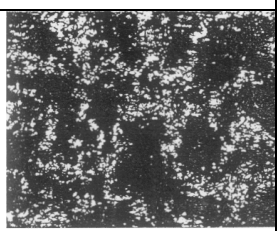

Fig. 5-b. Pictures taken from the optical microscope for the chemically treated surface (S5, S6 & S7).

At this moment, the saturation temperature at the measured pressure was compared to the pool temperature measured by the thermocouple. The vapor generated at the heated surface was condensed at the condenser where water was used as a cooling medium, and a constant system pressure was maintained by matching the rate of heat rejected at the condenser with the rate of heat added at the heated surface. The aforementioned procedure was repeated for each one of the tested plates with the tested fluids (demineralized water or acetone).

Reducing the heat flux in pre-determined steps by means of the variac from the highest value selected in the measurements of the pool boiling heat transfer coefficient. Sufficient time (about 30 minutes) was allowed to achieve steady state conditions after the power level was changed.

During all the tests, the saturation temperature was kept near 90°C (demineralized water) and 46°C (acetone) respectively. The average wall temperature was used to define the heat transfer coefficient; which equals the average value of the four wall thermocouples. The heat flux is based on the heated area of the tested plate surface.

3. Data reduction

For each power input, the heat transfer coefficient was calculated from the difference between the fluid bulk saturation temperature, and the average of the four plate wall temperatures, and tested plate heat flux as follows.

The heat flux q was determined from the separate measurements of the voltage and the current.

$$power\ input(Q) = I.\ V\cos\phi \quad Watt. \tag{4}$$

The useful power input Q_u was calculated by correcting the power input for the radial Q_r and the downward Q_d heat losses. The maximum radial and downward heat losses were estimated, therefore,

$$q = \frac{Q_u}{A} = \frac{IV\cos\varphi - Q_r - Q_d}{A} \quad W/m^2 \ . \tag{5}$$

The average wall temperature was corrected for the temperature drop within the aluminum wall thickness between thermocouples location and the upper boiling surface, therefore,

$$\overline{T}_w = \overline{T} - \frac{Q_u . \Delta X}{A.\ K\,alu} \quad ^oC, \tag{6}$$

where; A is the heating surface cross sectional area, $\overline{T}$ is the average value of the four wall thermocouple readings, $\overline{T}_w$ is the plate upper surface temperature, K_{alu} is the thermal conductivity of aluminum alloy 6061 (=167 W/m^oC) and Δx is the distance between the upper surface and the location of the thermocouple beads (= 0.005m).

From eqs. (4-6), the heat transfer coefficient (h) was obtained from the relation,

$$h=q/(\ \overline{T}_w\ -T_{sat}) \qquad (W/m^2\ ^oC). \tag{7}$$

4. Results and discussion

4.1. Heat transfer coefficient and enhancement

Fig. 6 shows the data taken for the seven tested plates with demineralized water and acetone, represented in double logarithmic scales of the heat transfer coefficient h as a function of the heat flux q. The diagrams show clearly two regions with different slopes of the heat transfer coefficient h. In the free convection region, the heat transfer coefficient h_{nc} increases moderately with the heat flux. It was proved both theoretically as well as experimentally by Gorenflo [14] that the slope in this region depends on whether free convection is laminar or turbulent. In the nucleate pool boiling region, the increase of h at all levels of heat flux for fully developed nucleate pool boiling can be seen for the various tested plates which is due to the agitation effect produced by the bubbles ascending from the nucleation sites on the heated surface. It is also noticed that for a specific heat flux with the various tested plates, the heat transfer coefficient for demineralized water is higher than that for acetone. This is because the acetone data indicate a larger ΔT_w in every case. This is most likely to occur because of the high wettability

of acetone, compared to the demineralized water. On roughened surface; the large cavities become flooded with liquid and higher superheats are needed to nucleate from the smaller cavities. Moreover, fig. 7 shows the same relation for both demineralized water and acetone data with the seven tested plates in two separate diagrams. It can be seen that for all levels of heat flux for the various plates, the data with roughened surfaces showed a significant improvement in heat transfer. It should be noted that the results for the constant system pressure may be approximately interpolated by a straight line. The slope of this line is different according to the surface condition-boiling liquid combination. It is also observed that for a specific heat flux or wall superheat, the heat transfer coefficient increases by increasing the microscopic roughness of the heated surface. The later result is clearly shown in fig. 8 for both demineralized water and acetone. Furthermore, in fig. 9, the present heat transfer coefficient data for the demineralized water and acetone with various roughened surfaces are normalized by the value of the smooth surface ($h^* = h/h_{S1}$) at constant heat flux of 10^5 W/m^2 against the surface roughness parameter R_p. It can be seen the significant enhancement of the normalized heat transfer coefficient h^* of the two tested fluids by increasing the microscopic roughness of the tested plates.

Fig. 10 reports the present data of the heat transfer coefficient as a function of the wall superheat ΔT_w for the various tested plates with demineralized water and acetone. It is observed that for a specific wall superheat, the heat transfer coefficient h increases by increasing the surface roughness. The results show an enhancement up to 600 % in the nucleate pool boiling heat transfer coefficient due to the variation in the roughness of the heated surface.

4.2. Size distribution function of the tested plates

In the present work, the distribution function of the active nucleation sites for the seven tested plates is estimated from the heat transfer measurements as follows:

The total heat flow rate Q leaving the heated surface in pool boiling consists of the heat flow rate by natural convection Q_{nc} and the heat flow rate produced by the nucleation boiling Q_{nuc}, thus;

$$Q = Q_{nc} + Q_{nuc} ,$$

or

$$q.A = q_{nc}.A_{nc} + q_{nuc}.A_{nuc} = q_{nc}\,(A - A_{nuc}) + q_{nuc}\,.\,A_{nuc},$$

where q_{nc} , q_{nuc} are the (natural convection and nucleate boiling) heat fluxes and A_{nc} , A_{nuc} are the pertaining areas on the heated surface. Dividing by the total area A and the wall superheat ΔT_w of the heated surface and rearranging yields,

$$h - h_{nc} = (h_{nuc} - h_{nc}).\ \frac{A_{nuc}}{A} \quad . \tag{8}$$

According to Han and Griffith [15], the area of influence of a single active site is πD_b^2, where; D_b is the diameter of the bubble when leaving the heated surface. Thus we obtain for all the N active sites;

$$A_{nuc} = N.\pi D_b^2 \ . \tag{9}$$

Using the experimental results for various refrigerants in turbulent natural convection, the heat transfer coefficient for h_{nc} can be calculated from eq. (10) ;

$$h_{nc} = 0.15 \left(\frac{g\,\beta`\,C`\,(\rho`\,\lambda`)^2\,\Delta T}{\eta`} \right)^{1/3} \quad . \tag{10}$$

Within the range of influence of the active nucleation sites, the transient conduction model introduced by Sakr [16] is applied, thus;

$$h_{nuc} = \frac{2}{\sqrt{\pi}} (\rho`C`\lambda`)^{0.5}.f^{0.5} \quad , \tag{11}$$

where f is the bubble frequency ($1/s$). According to McFadden and Grassmann [17], the bubble frequency;

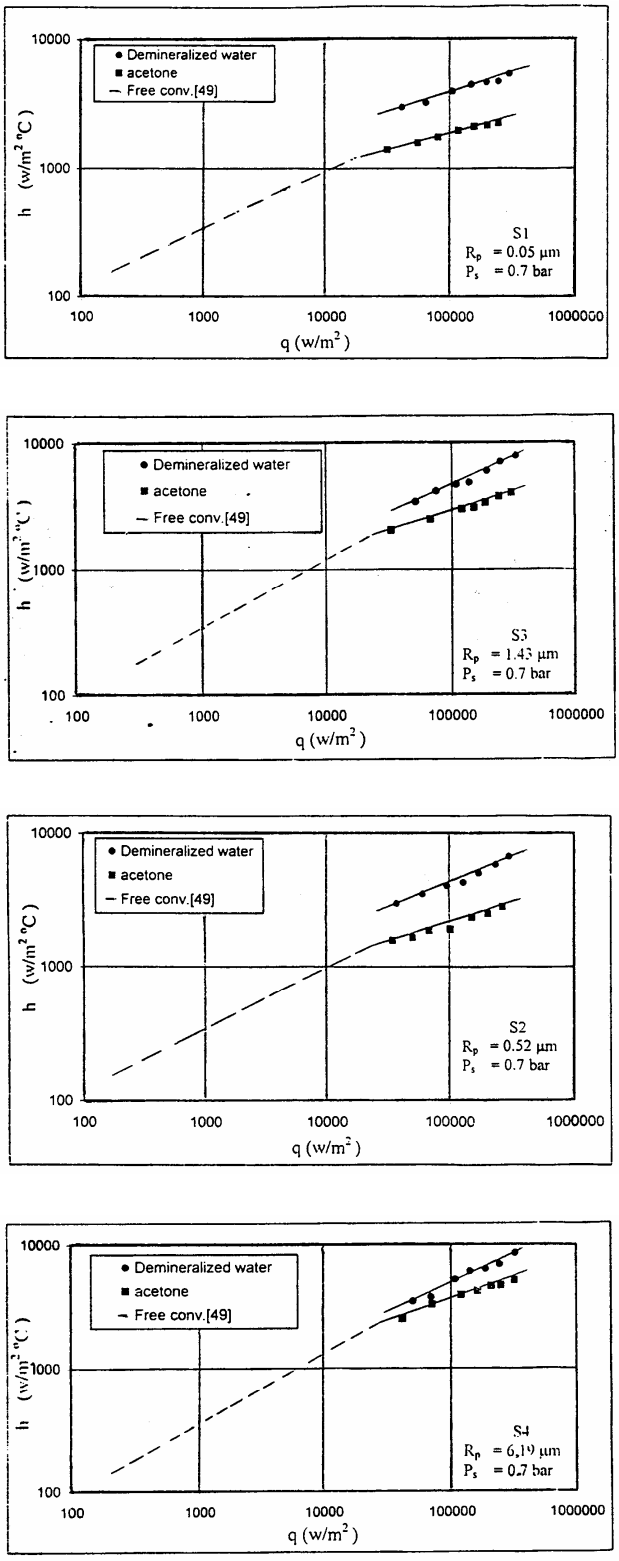

Fig. 6-a. Relation between pool boiling heat transfer coefficient and heat flux for mechanically treated surfaces.

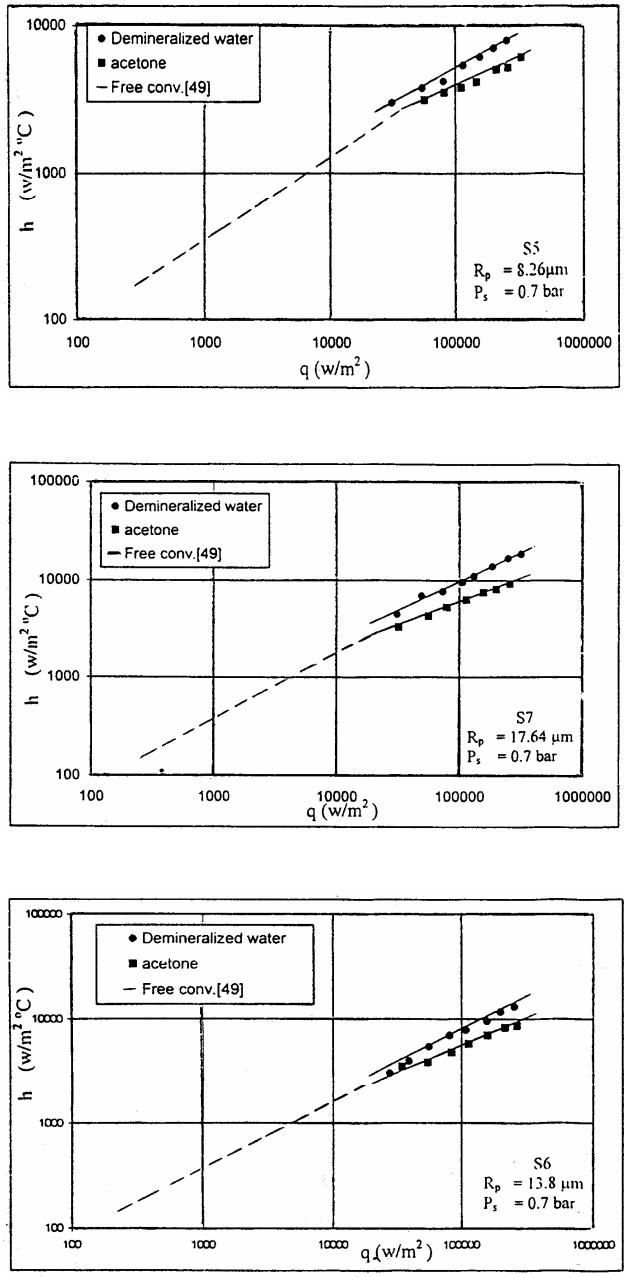

Fig. 6-b. Relation between pool boiling heat transfer coefficient and heat flux for chemically treated surfaces.

$$f^2.D_b^2 = 0.314 \frac{g(\rho` - \rho``)}{\rho`} . \quad (12)$$

Whereas the bubble diameter according to Fritz [18] ;

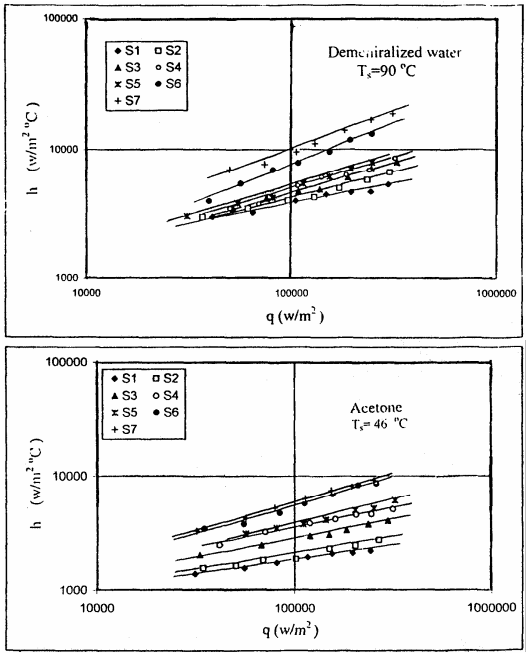

Fig. 7. Comparison between the pool boiling results of the seven tested surfaces using both demineralized water and acetone.

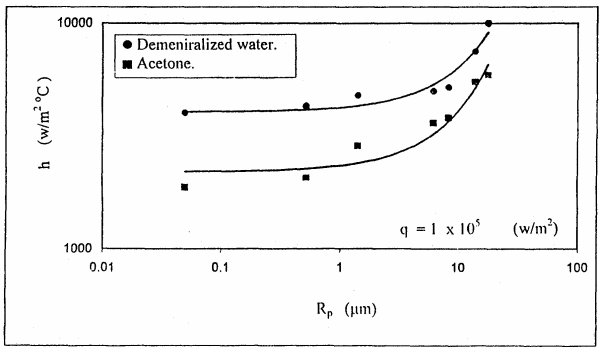

Fig. 8. Variation of pool boiling heat transfer coefficient with the surface roughness parameter.

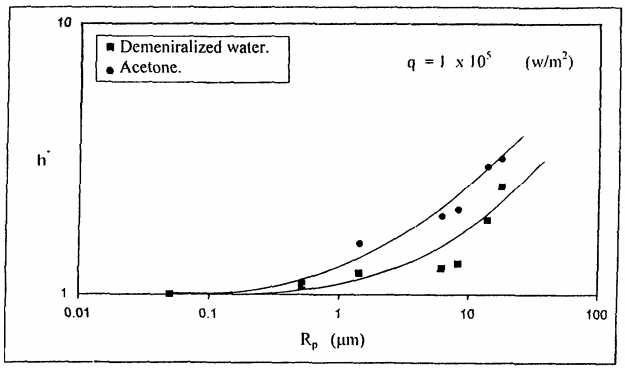

Fig. 9. Variation of normalized pool boiling heat transfer coefficient with the surface roughness parameter.

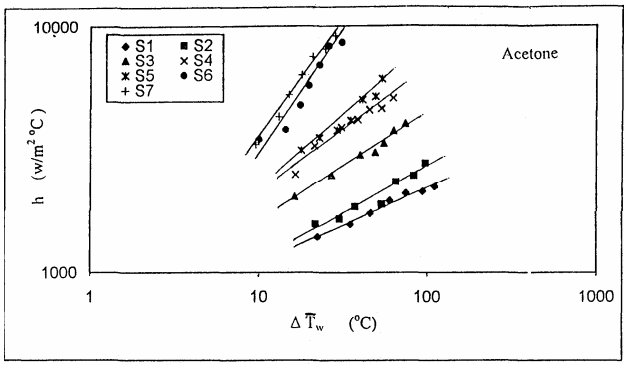

Fig. 10-a. Variation of pool boiling heat transfer coefficient with the wall superheat.

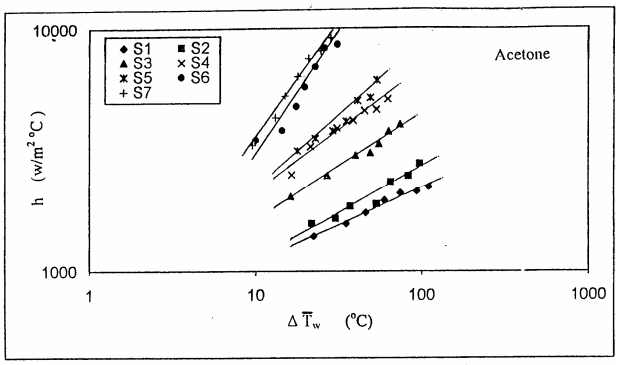

Fig. 10-b. Variation of pool boiling heat transfer coefficient with the wall superheat.

$$D_b = 0.0146\,\beta\left(\frac{2\sigma}{g(\rho`-\rho``)}\right)^{0.5} \quad . \qquad (13)$$

Here β is the contact angle which equals 35° for the refrigerants as suggested by Stephan [19]. Now, the number N of active nucleation sites can be calculated by eqs. (8-11) using the experimental values of h , ΔT_w and the thermophysical properties of the boiling liquid, in addition to the equations of f and D_b. Thus from eq. (8) ;

$$\frac{h - hnc}{hnuc - hnc} = \frac{N}{A}.\pi D_b^2 \quad .$$

On the other side, the minimum cavity radius r_c of a stable vapor bubble in a nucleation center activated at a given temperature difference ΔT is calculated from [8];

$$rc = \frac{2}{\Delta T}\left(\frac{\sigma\rho`}{(\rho`-\rho``)}\right)_{Tw} \cdot \left(\frac{Ts(v``-v`)}{\Delta h_v}\right)_{Tm} . \qquad (14)$$

The number N of active sites at a given superheat temperature ΔT comprises all nucleation sites emitting bubbles with radii $r \geq r_c$. Thus calculating N and r_c for different values of ΔT and plotting N versus r_c, one obtains the cumulative size distribution function $N(r)$, for the seven tested plates.

Fig. 11 shows the distribution functions $N(r)$ obtained in this way for the seven tested plates with demineralized water and acetone. It was found by trial and error that the interpolation lines in the diagrams of this figure may be expressed by exponential functions with a power term;

$$In\left(\frac{N}{A}\right) = \left(In\ \frac{N\ max}{A}\right) \cdot \left(1 - \left(\frac{r}{r\ st}\right)^{m}\right), \qquad (15)$$

where; N_{max}/A is the maximum value of N/A (at r=0), r_{st} is the maximum value of r which corresponds to the beginning of nucleation N/A=1 and m is an exponent.

Fig. 12 shows a comparison between the size distribution functions $N(r)$ for the various tested plates with demineralized water and acetone. It seems that, all the results indicate that as the minimum cavity radius r_c increases, the activated nucleation site density (N/A) decreases. This behavior is similar for the seven tested boiling sufaces with different

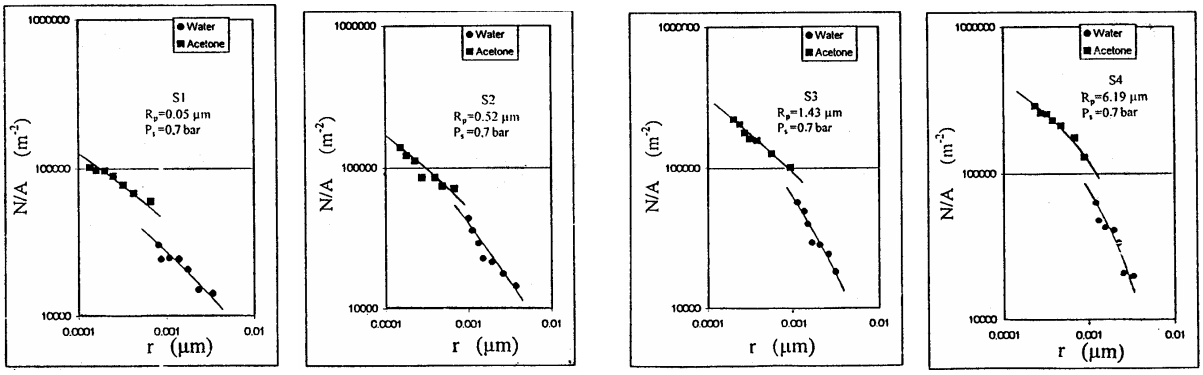

Fig. 11-a. Size distribution function for the four mechanically treated boiling surfaces.

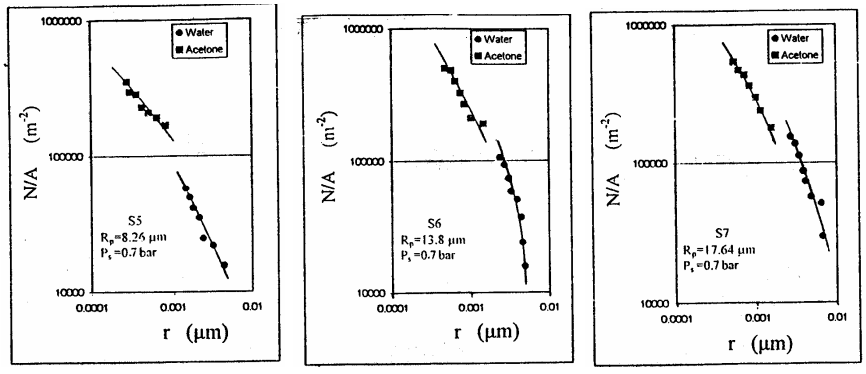

Fig. 11-b. Size distribution function for the three chemically treated boiling surfaces.

amounts depending on the value of R_p of each surface. Moreover, the small cavity is apparently more capable of holding a residual of vapor and is also able to be activated by its neighbors when boiling is initiated. Consequently, the performance of a heat transfer device in which vaporization occurs strongly depends on the roughness of the heated wall. Based on the thermophysical properties of the tested fluid, acetone is more likely to form nucleation sites than demineralized water. This phenomenon can be explained by the fact of the surface tension difference between the two fluids.

Fig. 13 depicts the variation in bubble nucleation flux rate *(N/A).f* as a function of heat flux (*q*) for the various tested plates with demineralized water and acetone. It is noticed that *(N/A).f* value increases by the increase in heat flux. This may be attributed to the fact that as the heat flux increases, a significant increase in the wall superheat is associated which tends to activate more nucleation sites on the heated surface at a specific roughness. This in turn, enhances the heat transfer process. It is also observed that for a specific fluid and constant heat flux, the *(N/A).f* value is increased by increasing the roughness of the heated surface. Again, *(N/A).f* also have a higher magnitude in acetone than in demineralized water. Moreover, fig. 14 shows the variation of *(N/A).f* with R_p at constant heat flux equals 2 x 10^5 W/m^2 for the various tested plates with demineralized water and acetone.

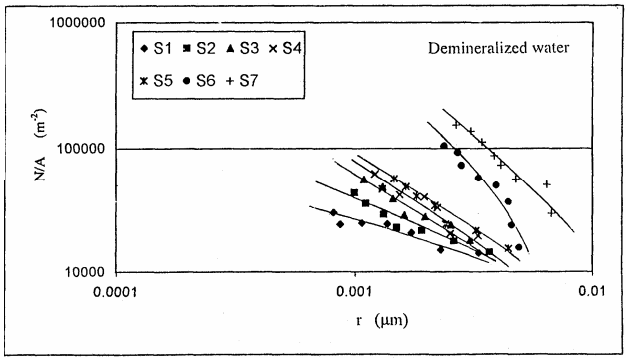

Fig. 12-a. Comparison between the size distribution functions of the seven tested boiling surfaces using deminaeralized water.

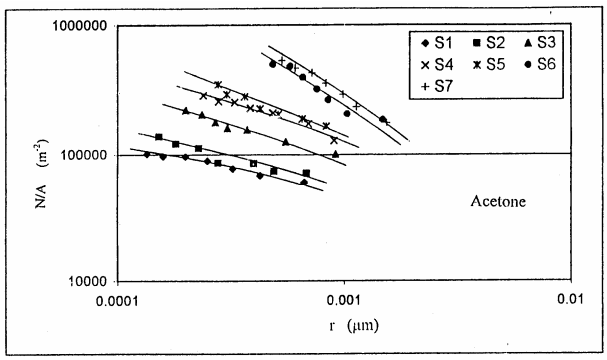

Fig. 12-b. Comparison between the size distribution functions of the seven tested boiling surfaces using acetone.

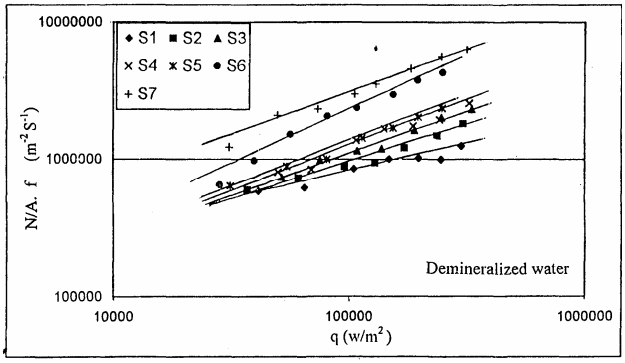

Fig. 13-a. Nucleate site density and frequency as a function of heat flux for the tested boiling surfaces using demineralized water.

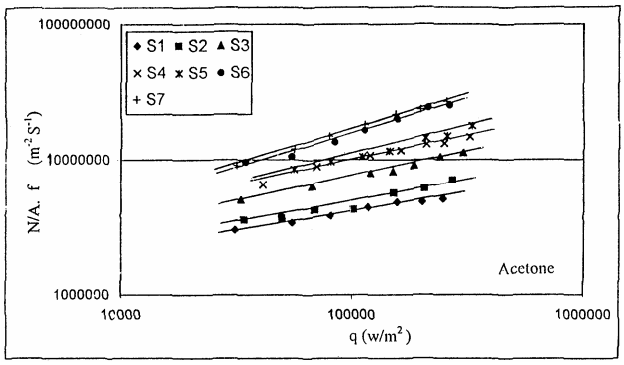

Fig. 13-b. Nucleate site density and frequency as a function of heat flux for the tested boiling surfaces using acetone.

In addition, the bubble nucleation flux rate *(N/A).f* for the various tested heated surfaces is normalized by the value of the smooth surface

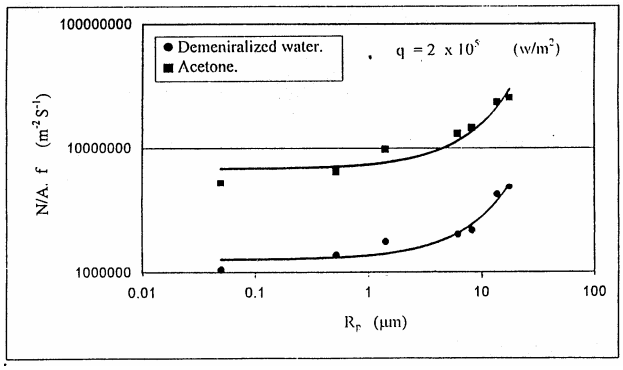

Fig. 14. Variation of nucleate site density and frequency with the surface roughness parameter.

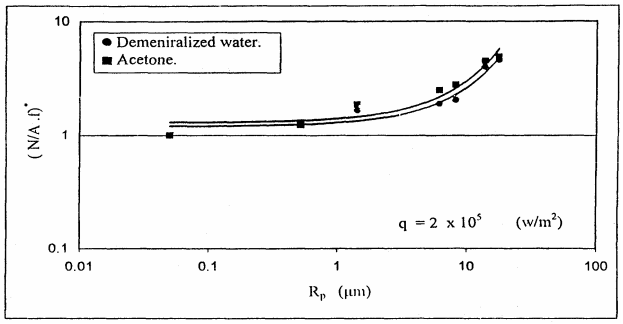

Fig. 15. Variation of the normalized nucleate site density and frequency with the surface roughness parameter.

$$(N/A.f)^* = \frac{(\frac{N}{A}.f)}{(\frac{N}{A}.f)_{S1}}$$ at heat flux equals 2 x 10^5 W/m^2 and is represented as function of R_p as shown in fig. 15. This figure reveals that within the entire investigated range of surface roughness, $(N/A).f)^*$ increases uniformly with increasing the roughness of the heated surface.

Generally, it is interesting to correlate the three-parametric size distribution function constants (N_{max}/A, r_{st} and m) with R_p. It must be mentioned that the constants (N_{max}/A, r_{st} and m) are deduced from the three parametric distribution functions (eq. (15)) calculated from the heat transfer measurements of the seven tested heated surfaces with demineralized water and acetone. Fig. 16 depicts the relation between the exponent m and the surface roughness parameter R_p. The results of refs. [8, 16] are presented for comparison. It seems that the exponent m of the present results is not

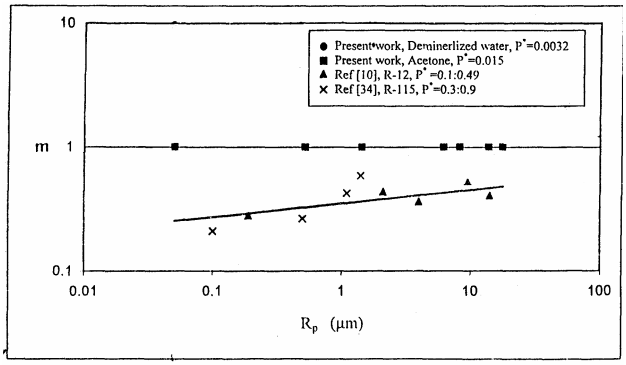

Fig. 16. Variation of the exponent m with the surface roughness parameter Rp.

affected by the roughness of the heated surface. It can be concluded that the exponent (m) may be considered as a constant equals unity. On the contrary, the previous results [8, 16] show different trend from the present results. It is believed that the reason for this difference may be due to the different surface treatment used in refs. [8, 16]. It must be mentioned that the authors of refs. [8, 16] used single mirror finish copper plate in their work, and after that they treated it mechanically with different grained emery papers (as in ref. [16]) or mechanically for some plates and chemically for the others (as in ref. [8]) to get heated surfaces with different surface finish. In addition to the different surface treatment, refs. [8, 16] boiled R-115 and R-11 (as in [8]) or R-12 (as in [16]) through extended pressure range. For this reason, their results for the exponent m seemed to increase with the surface roughness parameter R_p. Obviously, the present size and structure of the cavities strongly affects the influx of liquid from the pool drawn into the internal tunnel of the cavity.

Furthermore, fig. 17 shows the relation between the maximum bubble density N_{max}/A for the seven tested surfaces and the surface roughness parameter R_p. Again, The previous results of refs. [8, 16] are presented for comparison. It is observed from the present results that the maximum bubble density N_{max}/A increases by increasing R_p. This behavior is noted for both the demineralized water and acetone. This is perhaps due to the increase of the number of intersection points

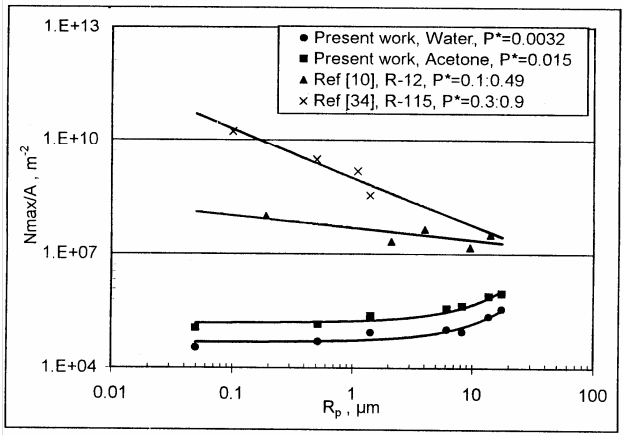

Fig. 17. Variation of the constant N_{max}/A with the surface roughness parameter Rp.

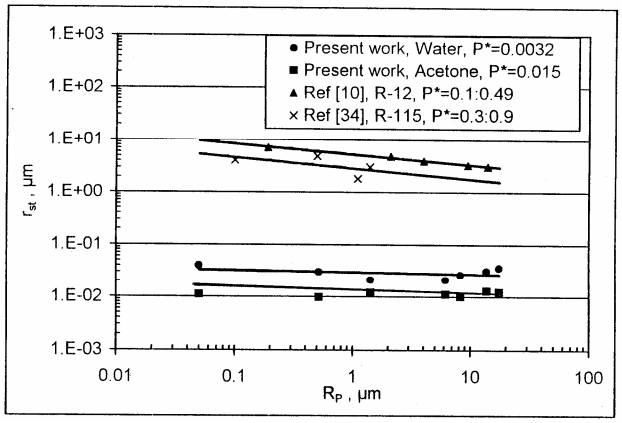

Fig. 18. Variation of the constant r_{sr} with the surface roughness parameter Rp.

per unit area of the heated surfaces (activated nucleation sites) as the surface roughness increases. This is also evidenced by the surface structure visualization showed in fig. 5. It is also observed that for a specific value of R_p, the N_{max}/A value of acetone is higher than that of demineralized water due to the surface tension difference between the two fluids. It is believed that acetone is able to activate more nucleation sites than demineralized water. On the contrary, the results of refs. [8, 16] showed a tendency of the maximum bubble density N_{max}/A to decrease with R_p. This may be due to the aforementioned reasons.

Finally, fig. 18 depicts the relation between the starting activated cavity radius r_{st} for the seven tested surfaces and R_p. The previous results of refs. [8, 16] are presented for comparison. It is observed from the present results that the starting activated cavity radius (r_{st}) decreases with the increase of R_P. This behavior holds for demineralized water and acetone. The decrease of the starting activated cavity radius r_{st} with R_p may be related to the nature of surface structure of the tested plates as evidenced by the structure visualization in fig. 5. Actually, this may be due to the fact that as the surface roughness increases the width of both longitudinal and perpendicular scratches also increases, so that the intersection area between two successive longitudinal and two successive perpendicular scratches becomes smaller which may lead to smaller values of r_{st} with R_p. On the other hand, the previous results of [8, 16] showed a similar trend in spite of the different method of surface treatment and different boiling liquids, in addition to the wide system pressure range that are used in their experiments.

The most interesting result is that the r_{st} values for demineralized water is higher than that for acetone. This is true for the present tested plates. This result supports the findings presented in figs. 10 and 16 and can be deduced from (h-q) relation, in addition to the size distribution function $N(r)$ for the present tested plates, in the sense that for a specific heat flux, the wall superheat ΔT_w associated with acetone is higher than that for demineralizated water. This activates more nucleation sites with smaller cavity radius in case of acetone than demineralized water. This fact may be explained by the higher values of N_{max}/A for acetone in comparison with those of demineralized water.

Generally, based on the present results, the three parameters N_{max}/A, r_{st} and m can be correlated with R_p in the form:

For demineralized water,

$$N_{max}/A = 155782\, e^{0.1109\, R_P}, \quad (17)$$

$$r_{st} = 0.0297\, (R_P)^{-0.0345} \quad . \quad (18)$$

For acetone,

$$N_{max}/A = 47722\, e^{0.1126\, R_P} \ , \quad (19)$$

$$r_{st} = 0.0108\, (R_P)^{-0.0044} \quad . \quad (20)$$

For both fluids,

$$m = 1. \quad (21)$$

5. Conclusions

Based on the present results, significant facts can be drawn as follows :

1. At constant system pressure, the absolute and normalized nucleate pool boiling heat transfer coefficients increase by the increase of the heat flux.
2. The absolute and normalized nucleate pool boiling heat transfer coefficients increase by increasing the roughness of the heated surface.
3. For a specific heat flux and constant system pressure, the absolute nucleate pool boiling heat transfer coefficient associated with demineralized water is higher than that of acetone.
4. For a specific wall superheat, the enhancement in the nucleate pool boiling heat transfer coefficient reaches up to 600 % due to the variation in the roughness of the heated surface.
5. The distribution function of the size of stable vapor bubbles in active nucleation sites of the heated surface may be expressed by exponential function with a power term (eq. (15)).
6. It is found that, the form of the size distribution function is affected by the roughness of the heated surface and the thermophysical properties of the boiling liquid (surface tension and viscosity).
7. For a specific wall superheat, acetone forms more nucleation sites than demineralized water.
8. For a specific surface roughness, the bubble nucleation flux rate $(N/A).f$ increases by increasing the heat flux.
9. For a specific heat flux, the bubble nucleation flux rate $(N/A).f$ increases by increasing the roughness of the heated surface.
10. The three-parameters for the tested heated surfaces N_{max}/A, r_{st} and m show a significant dependence on the surface roughness parameter R_p. It could be considered the exponent m is a constant equals unity. While N_{max}/A increases by increasing the roughness of the heated surfaces, and r_{st} decreases by increasing the roughness of the heated surface.
11. The parameters N_{max}/A, r_{st} and m can be correlated with the surface roughness parameter R_p as indicated in eqs. (16 to 20).

Nomenclature

A	Cross sectional area of the heated Surface, m^2,
C	Constant,
$C`$	Specific heat capacity, J/kg °C,
D	Bubble diameter, m,
f	Bubble frequency, 1/s,
g	Acceleration of gravity, m/s^2 ,
h	Heat transfer coefficient, W/m^2 °C,
Δh_v	Specific latent heat of vaporization, J/kg,
I	Current, ampere,
K	Constant,
K_{alu}	Thermal conductivity of aluminum alloy 6061, W/m°C,
m	Exponent,
N/A	Number of active nucleation sites per unit area, m^{-2} ,
N_{max}/A	Maximum value of the N/A (maximum bubble density), m^{-2} ,
N_o	Constant,
P	Saturation pressure, bar,
Q	Power, W,
Q_d	Downward heat loss, W,
Q_r	Radial heat loss, W,
Q_u	Upward heat supplied (actual power input), W,
q	Heat flux, W/m^2,
R_p	Surface roughness parameter defined by DIN 4762, µm ,
R_z	Surface roughness parameter defined , by Russian standard, µm,
rms	Surface roughness parameter defined by American standard, µm,
r	Bubble radius, µm,
r_c	Minimum radius of active nucleation sites, µm ,
r_{st}	Starting activated cavity radius, µm,
T	Fluid temperature , °C ,
ΔT_w	Excess temperature of the heated surface, °C ,
V	Voltage, volt
$V`, V``$	Specific volume of saturated liquid and Vapor, m^3/kg, and
ΔX	Wall thickness, m.
Greek symbols:	
β	Contact angle, degree,
$\overline{\beta}$	Volume expansion coefficient , 1/°C,
η	Dynamic viscosity, kg/m.s,
$cos\phi$	power factor,
ρ	Mass density, kg/m^3,

σ Surface tension, N/m and
λ Thermal conductivity , W/m°C.

Subscripts:

b Bubble at departure from heated surface ,
m Mean value,
s Saturation condition ,
w Wall condition,
nc At natural convection, and
nuc With the range of influence of nucleation site,

Superscripts:

` Saturated liquid ,
`` Saturated vapor,
* Function normalized by its value at the reference state and
– Mean value .

References

[1] M. Jakob, Heat Transfer, Vol. 1, Wiley, New York, pp. 631-642 (1949).

[2] P.J., Berenson, "Experiments on Pool Boiling Heat Transfer", Int. J. Heat and Mass Transfer, Vol. 5, pp. 985-999 (1962).

[3] G.N. Danilowa and A.V. Kupriyanova, "Heat Transfer", Soviet Res., ASME Publication, 2 ,79 (1970).

[4] G.N. Danilowa, "Heat Transfer", Soviet Res., ASME Publication, 2 , 73 (1970).

[5] C. Corty and A.S. Foust, "Surface Variables in Nucleate Boiling", AICHE Heat Transfer Conf., St. Louis, Mo (1953).

[6] C. Corty and A.S. Foust, "Surface Variables in Nucleate Boiling", Chem. Eng. Symb. Ser., Vol. 51 (16), pp. 1-12 (1955).

[7] Y. Tanes, "Influence of Surface Condition of the Heating Surface on Nucleate Boiling Heat Transfer", (ger.), Diss. Universität Karlsruhe (TH) (1976).

[8] M. Salem, Wärmeübergang beim Blasensieden Und Grössenver Teilungen Von Stabilen Blasenkeimen Sowie Von Rauhig Keit-Sverteilungen der Heizfläche, Diss, Universität Karlsruhe (TH) (1979).

[9] D. Anderson, R.L. Judd and H. Merte, , "Site Activation Phenomenon in Saturated Nucleate Boiling", Proc. ASME Joint Fluids England, Heat Transfer Symposium on the Role of Nucleation in Boiling and Cavitation, Detroit (1970).

[10] R.F. Gaertner, "Distribution of Active Sites in Nucleate Boiling of Liquids", Chem. Eng. Progress. Symp. Series, Vol. 59 (1963).

[11] W.T. Brown, Study of Flow Surface Boiling, Ph. D. Thesis, Mech. Eng. Dept., M.I.T (1967).

[12] S. Hsieh Weng and J. C. Chiou, "Nucleate Pool Boiling on Ribbed Surfaces With Micro-Roughness at Low and Moderate Heat Fluxes", Transactions of the ASME, Vol. 121, pp. 376-385 (1999).

[13] R.J. Benjamin and A.R. Balakrishnan, , "Nucleate Pool Boiling Heat Transfer of Pure Liquids at Low to Moderate Heat Fluxes", Int. J. Heat and Mass Transfer, Vol. 39, pp. 2495-2504 1996).

[14] D. Gorenflo, "Heat Transfer at Nucleate Boiling, Film Boiling and One-Phase Free Convection in a Wide Pressure Range", Abhandl. d. Deutschen Kältetechn. Vereins, Nr. 22, C.F. Müller-Verlag, Karlsruhe (1977).

[15] C.Y. Han and P. Griffith, "The Mechanism of Heat Transfer in Nucleate Pool Boiling", Int., J. Heat and Mass Trans. Vol. 8, pp. 887-914 (1965).

[16] H.S. Mohamed, , Effect of Surface Roughness on Pool Boiling Heat Transfer of R-12, M.Sc. Thesis, Zagazig Uni. Benha Branch, Shoubra Fac. of Eng., Cairo, Egypt (1984).

[17] P.W. McFadden, and P. Grassmann, "The Relation Between Bubble

[18] Frequency and Diameter During Nucleate Pool Boiling", Int. J. Heat and Mass Transfer, 5, 169 (1962).

[19] Fritz, W., 1935, "Maximum Volume of Vapor Bubbles", Zeitschrift Für Physik, Vol. 36, pp. 379-384.

[20] K. Stephan, Beitrag Zur Thermodynamik des Wärmeöergargs beim sieden, Abhandl. Deutscher Kältetechnischer Vereins, No. 18, C.F. Müller-Verlag, Karlsruhe, 19 (1964).

Received March 11, 2002
Accepted August 8, 2002